THE JOURNAL OF BIOLOGICAL CHEMISTRY Vol. 277, No. 18, Issue of May 3, pp. 16124–16130, 2002
Printed in U.S.A.

Crystallographic Studies of the *Escherichia coli* Quinol-Fumarate Reductase with Inhibitors Bound to the Quinol-binding Site*

Received for publication, January 25, 2002, and in revised form, February 15, 2002
Published, JBC Papers in Press, February 15, 2002, DOI 10.1074/jbc.M200815200

Tina M. Iverson‡§, César Luna-Chavez¶‖, Laura R. Croal‡‡, Gary Cecchini¶‖, and Douglas C. Rees‡§§**

From the ‡Division of Chemistry and Chemical Engineering, Howard Hughes Medical Institute, California Institute of Technology, Pasadena, California 91125, the ¶Molecular Biology Division 151-S, Department of Veterans Affairs Medical Center, San Francisco, California 94121, and the ‖Department of Biochemistry and Biophysics, University of California, San Francisco, California 94143, and the ‡‡Division of Biology, California Institute of Technology, Pasadena, California 91125

The quinol-fumarate reductase (QFR) respiratory complex of *Escherichia coli* is a four-subunit integral-membrane complex that catalyzes the final step of anaerobic respiration when fumarate is the terminal electron acceptor. The membrane-soluble redox-active molecule menaquinol (MQH_2) transfers electrons to QFR by binding directly to the membrane-spanning region. The crystal structure of QFR contains two quinone species, presumably MQH_2, bound to the transmembrane-spanning region. The binding sites for the two quinone molecules are termed Q_P and Q_D, indicating their positions proximal (Q_P) or distal (Q_D) to the site of fumarate reduction in the hydrophilic flavoprotein and iron-sulfur protein subunits. It has not been established whether both of these sites are mechanistically significant. Co-crystallization studies of the *E. coli* QFR with the known quinol-binding site inhibitors 2-heptyl-4-hydroxyquinoline-*N*-oxide and 2-[1-(*p*-chlorophenyl)ethyl] 4,6-dinitrophenol establish that both inhibitors block the binding of MQH_2 at the Q_P site. In the structures with the inhibitor bound at Q_P, no density is observed at Q_D, which suggests that the occupancy of this site can vary and argues against a structurally obligatory role for quinol binding to Q_D. A comparison of the Q_P site of the *E. coli* enzyme with quinone-binding sites in other respiratory enzymes shows that an acidic residue is structurally conserved. This acidic residue, Glu-C29, in the *E. coli* enzyme may act as a proton shuttle from the quinol during enzyme turnover.

The *Escherichia coli* quinol-fumarate reductase (QFR)[1] respiratory complex catalyzes the terminal step of anaerobic respiration when fumarate acts as the terminal electron acceptor (1). During this type of anaerobic respiration, electrons are donated to QFR by menaquinol (MQH_2) molecules in the membrane. The electrons are transferred to a covalently-bound flavin adenine nucleotide at the active site through three distinct iron-sulfur clusters and ultimately are used to reduce fumarate to succinate (2, 3). The QFR respiratory complex is composed of four polypeptide chains. Two of these chains, the flavoprotein (FrdA) and the iron protein (FrdB), comprise the soluble domain, which is involved in fumarate reduction, whereas the remaining two subunits (FrdC and FrdD) are membrane-spanning polypeptides involved in the electron transfer with quinones. High sequence identity between the soluble domain of the *E. coli* QFR and the soluble domain of succinate-quinone oxidoreductase (SQR, complex II) of the aerobic respiratory chain places these two complexes in the same family (4). Consistent with the sequence relationship, both enzymes from *E. coli* can bidirectionally catalyze the interconversion of succinate and fumarate (5), and each can functionally replace the other to support growth (6, 7). In contrast to the soluble domain, the transmembrane anchor subunits of the complex II family have little sequence identity and exhibit variable polypeptide and cofactor composition. Nevertheless, similar structural models for the membrane-spanning subunits have been proposed for the QFR and SQR respiratory complexes (8).

The structures of QFR respiratory complexes from *E. coli* (9) and *Wolinella succinogenes* (10) have been determined. Although these QFRs exhibit similar polypeptide-folds and cofactor arrangements in the soluble domain, there are distinctive features in the subunit organization and cofactor composition of the membrane-spanning domains. The structure of the QFR respiratory complex from *E. coli* (Fig. 1*A*) (9) contains two menaquinone molecules of unknown oxidation state designated Q_P and Q_D that are associated with the membrane-spanning region (Fig. 1*B*). Both of the binding sites for these quinol molecules had been predicted through a variety of techniques (11–15). Q_P is located near the [3Fe:4S] cluster of the soluble domain, whereas Q_D is positioned at the opposite side of the membrane. The minimum separation distance between the quinol rings of Q_P and Q_D is ~25 Å. (9). Although electron transfer has been observed to proceed at this distance (16), the

* This work was supported in part by the Department of Veterans Affairs (to G. C.), National Institutes of Health Grants GM61606 (to G. C.) and GM45162 (to D. C. R.), and National Science Foundation Grant MCB-9729778 (to G. C.). The costs of publication of this article were defrayed in part by the payment of page charges. This article must therefore be hereby marked "*advertisement*" in accordance with 18 U.S.C. Section 1734 solely to indicate this fact.

The atomic coordinates and structure factors (code 1KF6, 1KFY, and 1L0V) have been deposited in the Protein Data Bank, Research Collaboratory for Structural Bioinformatics, Rutgers University, New Brunswick, NJ (http://www.rcsb.org/).

§ Present address: Dept. of Biochemistry and Howard Hughes Medical Institute, MS 013, Brandeis University, Waltham, MA 02454.

** Present address: Center for Biophysics and Computational Biology, MC-147, University of Illinois at Urbana-Champaign, Urbana, IL 61801.

§§ To whom correspondence should be addressed: Division of Chemistry and Chemical Engineering, Howard Hughes Medical Institute, California Institute of Technology, MC 147-75CH, Pasadena, CA 91125. Tel.: 626-395-8393; Fax: 626-744-9524; E-mail: dcrees@caltech.edu.

[1] The abbreviations used are: QFR, quinol-fumarate reductase; MQH_2, menaquinol; SQR, succinate-quinone oxidoreductase; PEG, polyethylene glycol; HQNO, 2-heptyl-4-hydroxyquinoline-*N*-oxide; DNP-19, 2-[1-(*p*-chlorophenyl)ethyl]4,6-dinitrophenol.

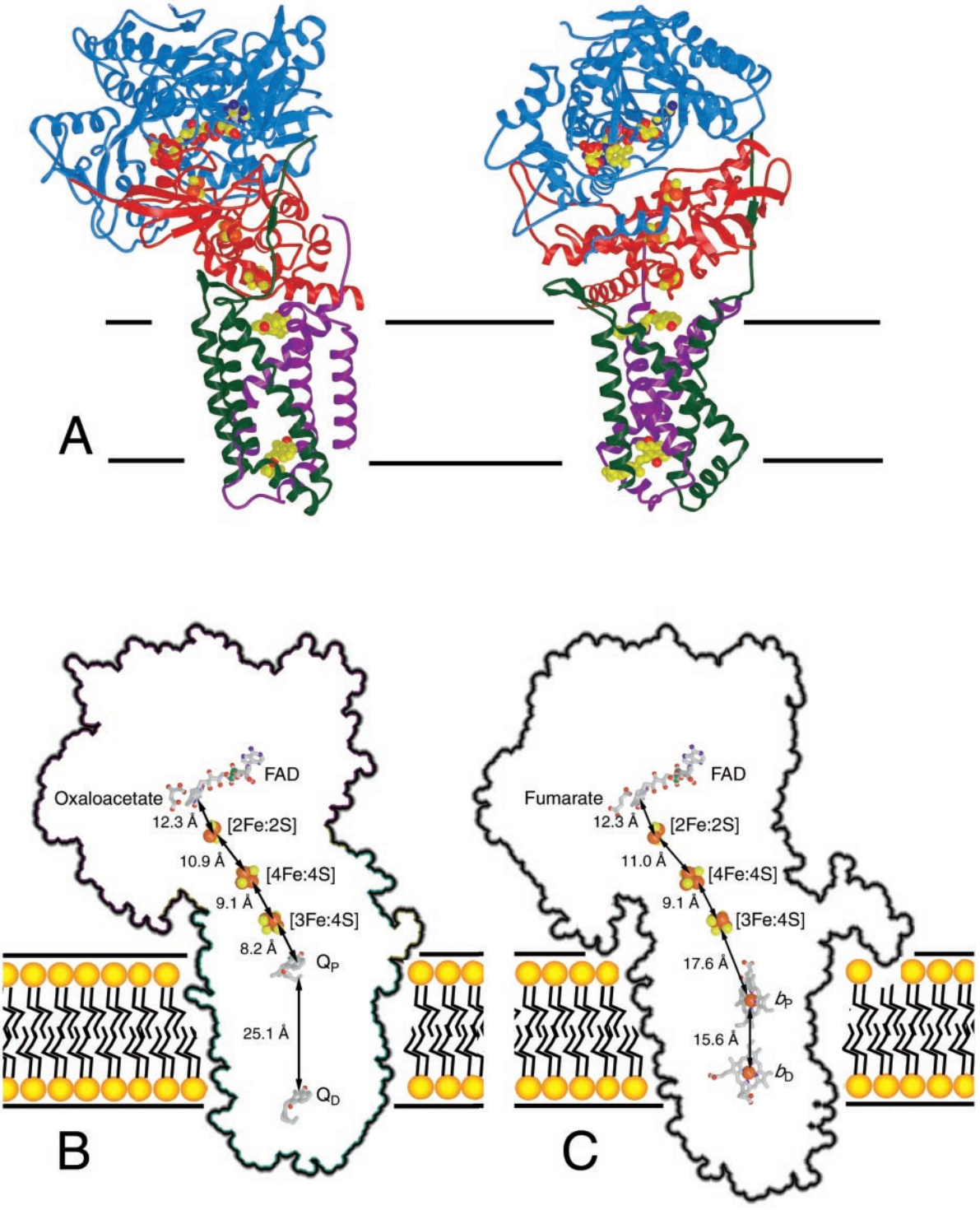

FIG. 1. **Polypeptide -fold and electron transfer distances in QFR.** *A*, *ribbon diagram views* of the *E. coli* QFR separated by a 90° rotation about a vertical axis. The flavoprotein is shown in *blue*, the iron protein is in *red*, and the transmembrane anchors are in *dark green* (FrdC) and *purple* (FrdD). The approximate boundary of the membrane is indicated with a *black line*. *B*, inter-cofactor distances of the *E. coli* enzyme. The known cofactors are superimposed onto an outline of the enzyme. *C*, inter-cofactor distances in the *W. succinogenes* enzyme. The *b*-type hemes associated with the membrane anchor reduce the electron transfer distance between a predicted distal quinol-binding site (data not shown). Figs. 1, 3, and 4 were made using Molscript (56), Bobscript (57), and Raster3D (58).

separation is much greater than the distance typically observed among redox cofactors that participate in physiological electron transfer (17). This raises the question of whether both quinol-binding sites are functionally relevant or whether quinol binding at the Q_D site fulfills a structural role. If intervening heme(s) were present between these two quinol-binding sites, as is the case in other members of the QFR/SQR family (3, 4), electron transfer would be expected to readily proceed from Q_D to the active site (Fig. 1*C*).

As quinone molecules are carriers of both protons and electrons, the transmembrane positioning of quinone (Fig. 2*A*)/quinol (Fig. 2*B*) molecules during oxidation and reduction can

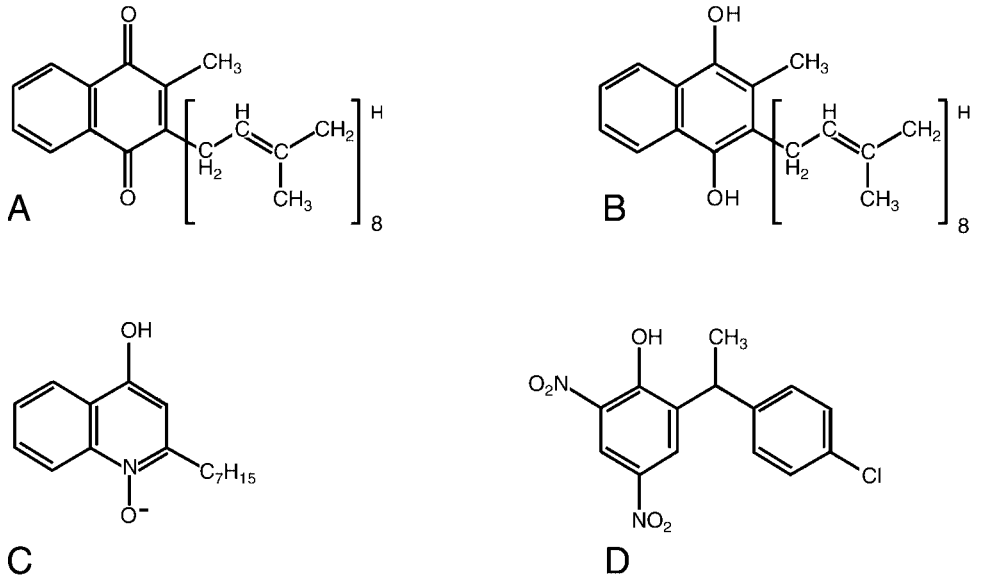

FIG. 2. **Chemical structures for oxidized menaquinone-8 (MQ-8) (*A*), reduced menaquinol-8 (*B*), HQNO (*C*), and DNP-19 (*D*).** MQ-8 is the primary menaquinone found in *E. coli* membranes, but smaller proportions of MQ-6, MQ-7, and MQ-9 are additionally present in the organism (59).

lead to proton translocation across the membrane exemplified by the Q-cycle mechanism employed by cytochrome bc_1 (18). It has been proposed that some fumarate reductases could participate in energy transduction if the oxidation of the quinol occurs at the Q_D site and is coupled to the reduction of a quinone positioned on the opposite side of the membrane in a second respiratory protein such as a hydrogenase or formate dehydrogenase (19). In the crystal structure of the two-heme QFR from *W. succinogenes* (10), a cavity search predicts that quinol molecules may bind at a site positioned similarly to Q_D (20, 21). The mutation of Glu-C66 near this cavity results in a loss of enzyme activity, whereas the protein retains a fully native structure (21), providing evidence that this location acts as a quinol-binding site. There is no evidence for a site positioned similarly to Q_P in the *W. succinogenes* complex; however, the presence of a Q_P site is not necessary for energy transduction when coupled to another respiratory complex.

To assess whether both the Q_D and the Q_P quinol-binding sites of the *E. coli* QFR respiratory complex are functionally relevant for electron transfer, the *E. coli* QFR respiratory complex has been co-crystallized with the known quinol-binding inhibitors 2-heptyl-4-hydroxyquinoline-*N*-oxide (HQNO) (Fig. 2*C*) and 2-[1-(*p*-chlorophenyl)ethyl] 4,6-dinitrophenol (DNP-19) (Fig. 2*D*), and the structures were determined at resolutions of 2.7 and 3.6 Å, respectively. Additionally, the native *E. coli* QFR structure has been further refined at 3.3 Å resolution for more accurate comparison to the inhibitor-bound forms. These studies demonstrate unequivocally that both inhibitors bind to the *E. coli* QFR at the Q_P site near the [3Fe:4S] cluster.

EXPERIMENTAL PROCEDURES

Protein Preparation and Crystallization—QFR was expressed and purified as previously described (22). All crystallizations were performed using a protein concentration of 30 mg/ml in 0.7% (w/v) of the polyoxyethylene detergent $C_{12}E_9$ (Thesit). Previously, optimal crystal formation occurred while using polyethylene glycol (PEG) 10,000 as the precipitant (9, 22); however, the variability between protein batches necessitated the use of different molecular weights of PEGs as the precipitant for each preparation. In this study, crystals grown using PEG 5000 monomethyl ether displayed the highest diffraction limit. Crystallization reactions were performed by the vapor diffusion method with hanging drops equilibrated over 12.5% PEG 5000 monomethyl ether, 85 mM magnesium acetate, 100 mM sodium citrate, pH 5.8, 100 μM EDTA, 0.001% dithiothreitol, and the appropriate inhibitor. Inhibitor concentrations were 100 μM HQNO (K_i = 0.2 μM) or 10 mM DNP-19 (K_i = 5.2 μM) (23, 24). Crystals grew in the orthorhombic space group $P2_12_12_1$ with unit cell dimensions listed in Table I. Prior to cryocooling, crystals were soaked in a solution containing 30% ethylene glycol and the crystallization components.

Structure Determination and Refinement—Data from co-crystals of QFR and HQNO were collected at 93 K at a wavelength of 1.00 Å on Stanford Synchrotron Radiation Laboratories (SSRL) beamline 9-2 using a Quantum 4 CCD detector, whereas data from co-crystals of QFR and DNP-19 were collected at a wavelength of 0.98 Å on SSRL beamline 9-1 using a MAR345 image plate detector. Data were processed using Denzo and Scalepack (25). As the structures are isomorphous, the structure of QFR bound to HQNO was refined following rigid body refinement of the original 3.3-Å resolution model (9) with the CNS program (26). The DNP-19 model was refined starting with the final model of HQNO bound to QFR after rigid body refinement. All models were built using the program O (27). Refinement was carried out using CNS (26) and REFMAC (28, 29). Tight non-crystallographic symmetry restraints were employed in regions of the molecule that exhibited similar electron densities but were released in crystal contacts and surface regions in which the structures of the two complexes clearly differed. Individual temperature factors were refined for the model of HQNO bound to QFR. For DNP-19 bound to QFR and the additional refinement performed on the previously reported native structure, group temperature factors were employed. The R_{free} was calculated for a test set of reflections identical to those used for the original structure determination with additional reflections randomly selected for the QFR + HQNO data set (Table I).

RESULTS

Binding of Quinone Inhibitors to the Membrane Anchor Subunits—Two of the most potent inhibitors of the reactions of *E. coli* QFR with quinones are HQNO (K_i = 0.2 μM) and DNP-19 (K_i = 5.2 μM) (23, 24). These inhibitors were chosen for co-crystallization studies with purified QFR to investigate their binding sites in the membrane domain of the enzyme. Crystallographic analysis of the binding of HQNO and DNP-19 to the *E. coli* QFR complex reveals density for both of these inhibitors at the Q_P site (Fig. 3 and Table I). HQNO is nearly isosteric with MQH_2 and binds at the Q_P site in a manner similar to that previously identified for MQH_2. Two hydrogen bond donors, Lys-B228 Nζ and Trp-D14 Nε are positioned within hydrogen-bonding distance of the negatively charged *N*-oxide (Fig. 4*A*). These two hydrogen bonds would satisfy the hydrogen bonding capabilities of menaquinone or semimenaquinone. The hydroxyl group on the other side of the HQNO ring is positioned

TABLE I
Data collection and refinement statistics

Numbers in parentheses indicate values for the highest resolution bin.

	Native	+HQNO	+DNP-19
Unit cell (Å)			
a	96.6	96.5	96.2
b	138.1	137.8	137.8
c	275.3	273.5	271.0
Resolution (Å)	50–3.3	50–2.7	50–3.6
No. of observations	219,456	292,370	124,660
Unique observations	49,332	93,174	38,919
R_{free} observations	1005	1953	819
Completeness (%)	87.2 (90.0)	91.6 (74.0)	91.1 (90.8)
R_{sym} [a]	0.093 (0.277)	0.063 (0.287)	0.104 (0.306)
I/σ	15.1 (6.3)	25.0 (6.2)	12.0 (4.1)
R_{cryst} [b]	0.245	0.231	0.264
R_{free}	0.290	0.280	0.301
root mean square deviation bond lengths	0.014	0.019	0.017
root mean square deviation bond angles	1.8 °	1.9 °	1.9 °
Q_P	MQ	HQNO	DNP
M	4σ	5σ	3σ
Q_D	MQ	–	–
PDB entry	1FUM, 1L0V	1KF6	1KFY
Wilson B (Å^2)	75	71	37

[a] $R_{sym} = \Sigma_i|I_i - \langle I\rangle|/\Sigma I_i$, where i is the "ith" measurement and $\langle I\rangle$ is the weighted mean of I.
[b] $R_{cryst} = \Sigma||F_{obs}| - |F_{calc}||/\Sigma|F_{obs}|$. R_{free} is the same as R_{cryst} for data omitted from refinement.

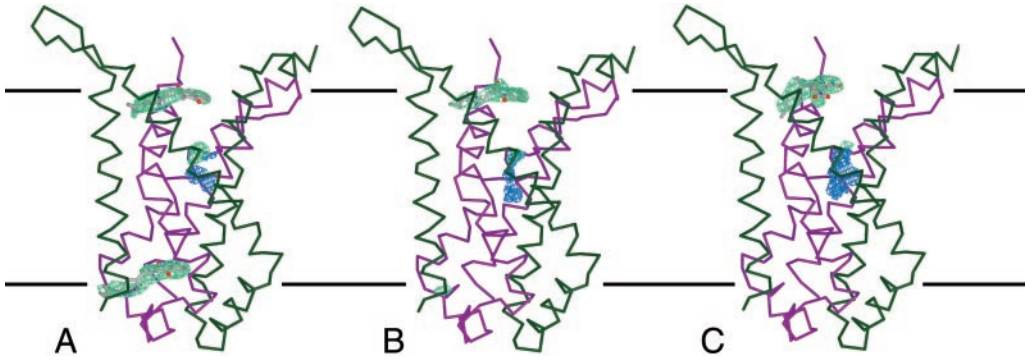

FIG. 3. **Binding of quinol and inhibitor molecules in the transmembrane-spanning region of the *E. coli* QFR.** The C_α trace of the membrane anchors is shown with the same coloring as in Fig. 1. The soluble domain of the complex has been omitted for clarity. Difference Fourier $|F_o| - |F_c|$ electron density (*green*) is contoured at 3σ and displayed at Q_P, Q_D, and M after molecules binding to those sites were omitted. Cavities calculated using the program VOIDOO (60) are displayed at the M site and are shown in *blue*. *A*, QFR at 3.3 Å resolution binds quinol molecules at both the Q_P and Q_D sites and additionally has density associated with the cavity M at the center of the membrane. *B*, QFR at 2.7 Å resolution shows clear density for an HQNO molecule bound at Q_P but lacks appreciable density at the Q_D site. The intensity of the density at position M has increased to 5σ. *C*, QFR at 3.6 Å resolution bound to DNP-19. Density at the Q_D site does not exceed background levels. Although the calculated cavity at the position M is larger, the density associated with it barely exceeds 3σ.

within hydrogen-bonding distance of the side chains of Glu-C29 Oϵ2 and Arg-D81 Nη1. Although DNP-19 also binds at the Q_P position, the binding site is shifted by over 2 Å with respect to HQNO or MQH_2 (Fig. 4*A*), and the inhibitor molecule only makes hydrogen-bonding contacts with one side of the quinol-binding pocket. The hydrogen bonds form between the DNP-19 O_2 and Lys-B228 Nζ and between the DNP-19 O13 and Trp-D14 Nϵ, whereas Glu-C29 and Arg-D81 do not make contacts. Significant positional differences between the QFR proteins in these structures are limited to the movement of the side chains of Gln-B225, Arg-C28, and Leu-C89 in the DNP-19-bound enzyme (Fig. 4*A*). These side chains would sterically clash with DNP-19 if they adopted the same conformation as exhibited in the other structures.

Kinetic analyses have established that HQNO is a non-competitive inhibitor of QFR, whereas DNP-19 acts as a pure competitive inhibitor (23, 24), and have suggested that both inhibitors bind at or near the same site. As the DNP-19 compound is not deeply inserted into Q_P but rather blocks the entrance to this site, this inhibitor probably acts by sterically preventing quinol from binding as predicted previously (23). Neither inhibitor was observed to bind to the Q_D site; yet intriguingly, electron density for Q_D, which was strong in the 3.3 Å resolution structure determination, is absent when either HQNO or DNP-19 is bound to the Q_P-binding site (Fig. 3).

Unassigned Density in the Membrane-spanning Domain—In the 3.3-Å resolution structure containing MQH_2 bound at both the Q_P and Q_D positions, an unassigned feature in the electron density with a height of 4σ above background was visible between these two sites (Fig. 3*A*). This extra density, designated "M," coincides with the only major cavity found in the *E. coli* QFR structure. The density in this location is additionally present in the inhibitor structures (Fig. 3, *B* and *C*) and becomes stronger with improved resolution, reaching 5σ in the HQNO co-structure. For comparison, the omission of the HQNO inhibitor from the HQNO co-structure results in a difference Fourier density of 5.8σ, whereas the omission of the quinone molecules bound at Q_D and Q_P from the 3.3-Å resolution structures result in difference Fourier densities of 4.5σ and 3.9σ, respectively. It is possible that this additional density at M represents a partially ordered cofactor that has not been previously detected. The distance between the M site and each of the other established quinol-binding sites is ~13 Å. The side chains near the density (Fig. 4*B*) associated with this cavity

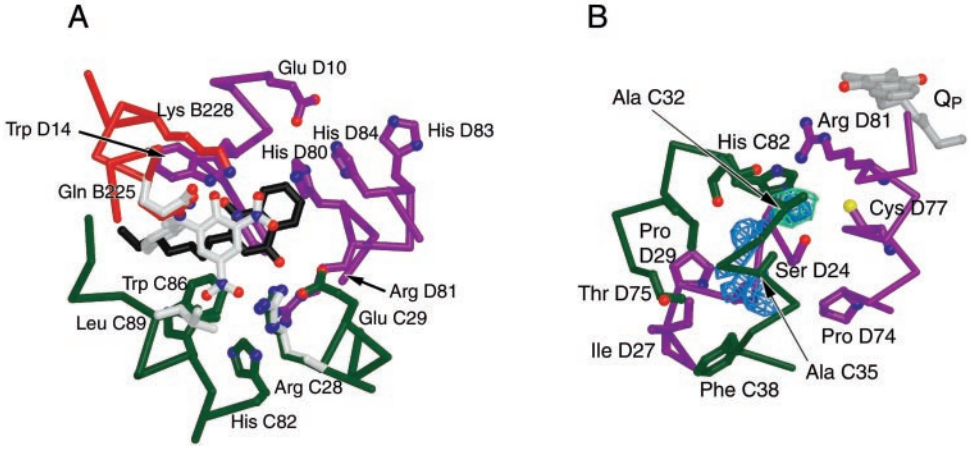

FIG. 4. **Comparison of inhibitors binding at Q_P and side chains surrounding the M site.** *A*, comparison of inhibitor-binding position and side chain movements. Residues from FrdB have the carbon atoms colored in *red*, residues from FrdC have the carbon atoms colored in *dark green*, whereas residues from FrdD have the carbon atoms colored in *purple*. Oxygen atoms are colored in *red*, nitrogen atoms are *blue*, and sulfur atoms are in *yellow*. The inhibitor HQNO has the carbon atoms colored in *black*, whereas the inhibitor DNP-19 has the carbon atoms colored in *white*. The orientation of the view is looking onto the Q_P-binding site from the surface of the membrane. The side chain positions are taken from the QFR structure with HQNO bound (Protein Data Bank code 1KF6) and are within the error of the side chain positions from the structure of QFR with MQ bound (Protein Data Bank code 1FUM). The differences in side chain position between the DNP-19 bound enzyme and the other two structures that were greater than the error of the determined structures were limited to Gln-B225, Arg-C28, and Leu-C89. The altered positions of these three side chains that allow for DNP-19 binding are shown with the carbon atoms in *white*. *B*, the position M from the structure bound to HQNO with surrounding side chains. The orientation of the molecule in this view is the same as in Fig. 3*B*. The approximate location of a binding site can be inferred from a cavity calculated using the program VOIDOO (60) (*cyan*) and difference Fourier ($|F_o| - |F_c|$) electron density contoured at 3σ (*green*). The coloring of atoms is the same as seen in Fig. 4*A*. The position of the quinone at Q_P is taken from the QFR structure with quinones bound (Protein Data Bank code 1L0V), and the quinone molecule is shown with the carbon atoms colored in *gray*.

tend to be polar, whereas those in the region not associated with any density tend to be apolar, giving this cavity the hydrophobicity characteristics of a quinone-binding site. Site-directed mutagenesis suggests that the residues lining this location are critical for enzyme function (14). However, the location of this density in the center of the membrane would be unusual for a quinol-binding site when compared with those structurally characterized to date. The binding of a metal ion at this site is also unlikely, because neighboring residues appear too distant to act as metal ligands and no significant peaks are observed near this site in anomalous difference Fourier maps. Thus, the identity of the species at this M site cannot be determined at present.

DISCUSSION

Mechanistic Role for the Q_P-binding Site—Q_P is positioned ~8 Å from the [3Fe:4S] cluster, implicating this quinol-binding site as the immediate electron donor to the redox cofactors in the soluble domain. The fully reduced quinol bound at Q_P must release two electrons and two protons during oxidation to the quinone. As the [3Fe:4S] cluster is a one electron acceptor, QFR must be able to stabilize both the fully reduced quinol and at least transiently the semiquinone oxidation states at the Q_P-binding site during turnover. The binding of HQNO to the Q_P site strengthens the hypothesis that the semiquinone form can be stabilized at this site (15), because HQNO is proposed to be a mimic of the semiquinone intermediate.

In both the QFR structure with HQNO bound at Q_P and the structure with MQH_2 bound, the side chain of Glu-C29 lies within hydrogen-bonding distance of the hydroxyl of the HQNO or MQH_2 ring. The proximity of the Glu-C29 residue and the fact that the HQNO elicits a significant change in the EPR line shape of the [3Fe:4S] cluster (30) are consistent with HQNO binding near the Q_p site (Fig. 3). The obligatory presence of an acidic residue near the exchangeable quinone-binding site is emerging as a theme in respiratory proteins. The Q_i ubiquinone-binding site of cytochrome bc_1 (31–33) contains the conserved Asp-229 (chicken numbering) residue within hydrogen-bonding distance of the ubiquinone. Similarly, the proposed ubiquinol-binding site in quinol oxidase (34) contains a conserved Asp-75, and the co-structures of cytochrome bc_1 with the Q_o-binding inhibitor stigmatellin shows that Glu-272 of the cytochrome *b* subunit lies within hydrogen-bonding distance of stigmatellin (35). In the *W. succinogenes* QFR, Glu-C66 has been shown to be an essential component of the menaquinol oxidation site (21), whereas in the *Bacillus subtilis* SQR, the conserved Asp-C52 is part of the predicted HQNO-binding site (36). Additionally, in the *Paracoccus denitrificans* SQR, the mutation of Asp-D88 to a glycine confers resistance to the known quinone-binding inhibitor carboxin (37). In eukaryotes, the small membrane anchor (FrdD/SdhD/cyt b_S) gene of QFR/SQR (38–41) contains three conserved aspartate residues, and the alteration of one, Asp-92 (human numbering of uncleaved sequence), is associated with hereditary paraganglioma (42). Site-directed mutagenesis (43) and azido-^{3}[H]-linked quinone labeling (40) predicts that Asp-92 is located within a region important for ubiquinone binding.

Because variants of cytochrome bc_1 altering Glu-272 of the cytochrome *b* subunit impair enzyme turnover while maintaining ubiquinol binding to Q_o (35), Glu-272 is proposed to participate in proton shuttling rather than be involved in stabilizing the binding of a protonated quinone species. Similarly, in the soluble quinohemoprotein amine dehydrogenase from *Pseudomonas putida*, Asp-33γ is presumed to be the proton shuttle (44) for the covalently attached cysteine tryptophylquinone. Although the photosynthetic reaction center does not contain an acidic residue that directly hydrogen-bonds to the ubiquinone, two acidic residues in *Rhodobacter sphaeroides* reaction center, Glu-L212 and Asp-L213, are located within 5 Å of the semiquinone bound at Q_B (45) and have been implicated as proton shuttles (46). A role with the carboxyl group primarily involved in proton transfer is consistent with the EPR analysis of the FrdC E29L variant of the *E. coli* QFR (15).

Quinol molecules have two hydroxy groups located on opposite sides of the molecule (Fig. 2); each is deprotonated during oxidation. As discussed above, the acidic residue Glu-C29 may act as the proton shuttle during quinol oxidation. In cyto-

chrome bc_1 (both Q_i and Q_o), ubiquinol oxidase and the *W. succinogenes* QFR, a conserved histidine residue is located on the opposite side of the quinone-binding site from the acidic residue. Because the photosynthetic reaction center quinone-binding site also contains a conserved histidine residue (His-L190), searches for consensus quinone-binding sequences have focused on conserved histidine residues (47). The *E. coli* QFR departs from the use of a histidine in the quinol-binding site. Although several histidine side chains are near the Q_P site and may therefore act as secondary proton shuttles in a chain from Glu-C29 (Fig. 4*A*), none of them is optimally positioned to form hydrogen bonds with the quinol hydroxyl groups. Instead, on the opposite side of the quinol, DNP-19, and HQNO molecules from Glu-C29, all of these molecules are positioned within hydrogen-bonding distance of Trp-D14 Nϵ and Lys-B228 Nζ that could participate in the proton transfer pathway. By analogy to the photosynthetic reaction center in which the quinone bound at the Q_B site undergoes a propeller twist during reduction (45), multiple positions of the quinone may also be utilized in QFR to generate additional contacts with residues involved in the proton shuttle.

In addition to HQNO and DNP, the other known inhibitors of the *E. coli* QFR have been either shown or predicted to bind to the Q_P site (15, 24), and the available kinetic data are consistent with a single dissociable binding site in the QFR complex (24, 48). Furthermore, although the *E. coli* QFR is insensitive to many of the other known complex II quinone-binding inhibitors, the locations of mutations that confer resistance to carboxin and 2-thenoyltrifluoroacetone in the single heme containing *P. denitrificans* SQR (37, 49) suggest that both of these inhibitors bind at a site positioned similarly to Q_P. Thus, the insensitivity of the *E. coli* QFR to these inhibitors does not reflect the binding of these inhibitors to a non-functional site.

The M-binding Site—Three molecules of ubiquinone have recently been proposed to bind specifically to the two quinone-binding sites, Q_i and Q_o, of cytochrome bc_1 respiratory complex (50). One molecule is proposed to bind at the ubiquinone reduction center, Q_i, whereas two are proposed to bind at the ubiquinol oxidation site, Q_o. In the *E. coli* QFR structure, the entity at the M site is separated from Q_P by the side chain of Arg-D81 (Fig. 4*B*). Thus, the double occupancy model proposed for the cytochrome bc_1 Q_o site (50, 51) would require an alternative position for the side chain of Arg-D81. The position of Arg-D81 on an α-helix and facing in toward the center of the protein would make it difficult for this side chain to move out of the pocket into solvent, constraining any repositioning relative to the M cavity. Although it seems more likely that M is a separate entity from Q_P, the rearrangement of Arg-D81 to form a larger binding pocket cannot be entirely ruled out.

The Q_D-binding Site—Quinol oxidation at the Q_D site of the *E. coli* QFR has not been demonstrated. However, one intriguing aspect of the QFR structures with inhibitor bound at the Q_P site is that no density corresponding to quinol bound at Q_D is observed. In the cytochrome bc_1 complex, the binding of either of the inhibitors stigmatellin or methoxyacrylate stilbene at Q_o reduces the affinity for the inhibitor or quinol at the second Q_o site in the dimer (52). As a result of the anti-cooperative binding behavior, these two compounds can inhibit the cytochrome bc_1 complex with a stoichiometry of 0.5 molecules of inhibitor/Q_o-binding site. In the *E. coli* QFR, the absence of quinol density at Q_D when an inhibitor is tightly associated at Q_P could suggest a similar anti-cooperative behavior in these binding sites. Although the native structure of QFR containing only quinones bound shows density at both Q_P and Q_D (9), the density at Q_P is much weaker. This finding may reflect a disorder in quinol binding or it may reflect partial occupancy of the site or both. Although the experiments presented here cannot establish the functional relevance of Q_D, the observation that the occupancy at the Q_D site decreases in the structures with inhibitors bound to the Q_P site indicates that the binding of a quinone species at the Q_D site is not required for protein stability.

Electron Transfer during Catalysis—QFRs and SQRs exhibit variability in membrane subunit composition, heme content, and quinol/quinone association, suggesting that electron transfer through the membrane-spanning region differs between the various enzymes of this family. The experiments on many heme-containing members of the QFR/SQR family have yielded evidence for the participation of a site positioned similarly to Q_D during electron transfer (21, 40, 43, 53); however the molecular characteristics of these functional sites resemble those observed in Q_P in the *E. coli* QFR-respiratory complex. Quinol oxidation at a site positioned similarly to Q_D indicates that transmembrane electron transfer occurs and would be obligatory for the generation of a transmembrane electrochemical potential gradient during turnover (54, 55). The existence of the M site near the middle of the membrane possibly identifies an additional center that could participate in an electron transfer pathway between Q_P and Q_D in the *E. coli* QFR. A more definitive proposal for the mechanistic role of Q_D during catalysis by the *E. coli* QFR will require determination of whether the non-functional mutants generated at the Q_D and M positions retain the native structure and identification of the molecular species at the M site.

Acknowledgments—We thank A. P. Yeh, R. B. Bass, and A. Dunn for experimental assistance, H. Miyoshi for generously providing the DNP-19 inhibitor compound, Y. F. C. Lau for providing sequences of the mouse SQR before publication, C. L. Drennan and D. Ringe for the use of computer facilities, and T. Ohnishi, I. Schröder, P. L. Dutton, H. B. Gray, and R. A. Marcus for enlightening discussions.

REFERENCES

1. Gottschalk, G. (1986) *Bacterial Metabolism*, 2nd Ed, Springer-Verlag New York Inc., New York
2. Kröger, A., Geisler, V., Lemma, E., Theis, F., and Lenger, R. (1992) *Arch. Microbiol.* **158,** 311–314
3. Ackrell, B. A. C., Johnson, M. K., Gunsalus, R. P., and Cecchini, G. (1992) in *Chemistry and Biochemistry of Flavoenzymes* (Müller, F., ed) Vol. 3, pp. 229–297, CRC Press, Inc., Boca Raton, FL
4. Hägerhäll, C. (1997) *Biochim. Biophys. Acta* **1320,** 107–141
5. Pershad, H. R., Hirst, J., Cochran, B., Ackrell, B. A. C., and Armstrong, F. A. (1999) *Biochim. Biophys. Acta* **1412,** 262–272
6. Guest, J. R. (1981) *J. Gen. Microbiol.* **122,** 171–179
7. Maklashina, E., Berthold, D. K., and Cecchini, G. (1998) *J. Bacteriol.* **180,** 5989–5996
8. Hägerhäll, C., and Hederstedt, L. (1996) *FEBS Lett.* **389,** 25–31
9. Iverson, T. M., Luna-Chavez, C., Cecchini, G., and Rees, D. C. (1999) *Science* **284,** 1961–1966
10. Lancaster, C. R. D., Kröger, A., Auer, M., and Michel, H. (1999) *Nature* **402,** 377–385
11. Ruzicka, F. J., Beinert, H., Schepler, K. L., Dunham, W. R., and Sands, R. H. (1975) *Proc. Natl. Acad. Sci. U. S. A.* **72,** 2886–2890
12. Salerno, J. C., Harmon, H. J., Blum, H., Leigh, J. S., and Ohnishi, T. (1977) *FEBS Lett.* **82,** 179–182
13. Westenberg, D. J., Gunsalus, R. P., Ackrell, B. A. C., and Cecchini, G. (1990) *J. Biol. Chem.* **265,** 19560–19567
14. Westenberg, D. J., Gunsalus, R. P., Ackrell, B. A. C., Sices, H., and Cecchini, G. (1993) *J. Biol. Chem.* **268,** 815–822
15. Hägerhäll, C., Magnitsky, S., Sled, V. D., Schröder, I., Gunsalus, R. P., Cecchini, G., and Ohnishi, T. (1999) *J. Biol. Chem.* **274,** 26157–26164
16. Winkler, J. R., DiBilio, A., Farrow, N. A., Richards, J. H., and Gray, H. B. (1999) *Pure Appl. Chem.* **71,** 1753–1764
17. Page, C. C., Moser, C. C., Chen, X., and Dutton, P. L. (1999) *Nature* **402,** 47–52
18. Mitchell, P. (1961) *Nature* **191,** 144–148
19. Ohnishi, T., Moser, C. C., Page, C. C., Dutton, P. L., and Yano, T. (2000) *Structure* **8,** R23–R32
20. Iverson, T. M., Luna-Chavez, C., Schröder, I., Cecchini, G., and Rees, D. C. (2000) *Curr. Opin. Struct. Biol.* **10,** 448–455
21. Lancaster, C., Groβ, R., Haas, A., Ritter, M., Mantele, W., Simon, J., and Kroger, A. (2000) *Proc. Natl. Acad. Sci. U. S. A.* **97,** 13051–13056
22. Luna-Chavez, C., Iverson, T. M., Rees, D. C., and Cecchini, G. (2000) *Protein Expression Purif.* **19,** 188–196
23. Yankovskaya, V., Sablin, S. O., Ramsay, R. R., Singer, T. P., Ackrell, B. A. C., Cecchini, G., and Miyoshi, H. (1996) *J. Biol. Chem.* **271,** 21020–21024
24. Maklashina, E., and Cecchini, G. (1999) *Arch. Biochem. Biophys.* **369,** 223–232
25. Otwinowski, Z. (1993) in *CCP4 Study Weekend Data Collection and Processing*

(Sawyer, L., Isaacs, N., and Bailey, S., eds), pp. 56–62, SERC Daresbury Laboratory, Daresbury, UK
26. Brünger, A., Adams, P., Clore, G., DeLano, W., Gros, P., Grosse-Kunstleve, R., Jiang, J., Kuszewski, J., Nilges, M., Pannu, N., Read, R., Rice, L., Simonson, T., and Warren, G. (1998) *Acta Crystallogr. Sec. D* **54,** 905–921
27. Jones, T. A., Zou, J. Y., Cowan, S. W., and Kjeldgaard, M. (1991) *Acta Crystallogr. Sec. A* **47,** 110–119
28. Bailey, S. (1994) *Acta Crystallogr. Sec. D* **50,** 760–763
29. Murshudov, G. N., Vagin, A. A., and Dodson, E. J. (1997) *Acta Crystallogr. Sec. D* **53,** 240–255
30. Rothery, R. A., and Weiner, J. H. (1998) *Eur. J. Biochem.* **254,** 588–595
31. Xia, D., Yu, C., Kim, H., Xia, J., Kachurin, A. M., Zhang, L., Yu, L., and Deisenhofer, J. (1997) *Science* **277,** 60–66
32. Iwata, S., Lee, J. W., Okada, K., Lee, J. K., Iwata, M., Rasmussen, B., Link, T. A., Ramaswamy, S., and Jap, B. K. (1998) *Science* **281,** 64–71
33. Zhang, Z. (1998) *Nature* **392,** 677–684
34. Abramson, J., Riistama, S., Larsson, G., Jasaitis, A., Svensson-Ek, M., Laakkonen, L., Puustinen, A., Iwata, S., and Wikström, M. (2000) *Nat. Struct. Biol.* **7,** 910–917
35. Crofts, A. R., Barquera, B., Gennis, R. B., Kuras, R., Guergova-Kuras, M., and Berry, E. A. (1999) *Biochemistry* **38,** 15807–15926
36. Smirnova, I. A., Hägerhall, C., Konstantinov, A. A., and Hederstedt, L. H. (1995) *FEBS Lett.* **359,** 23–26
37. Matsson, M., and Hederstedt, L. (2001) *J. Bioenerg. Biomembr.* **33,** 99–105
38. Bullis, B. L., and Lemire, B. D. (1994) *J. Biol. Chem.* **269,** 6543–6549
39. Saruta, F., Hirawake, H., Takamiya, S., Ma, Y., Aoki, T., Sekimizu, K., Kojima, S., and Kita, K. (1996) *Biochim. Biophys. Acta* **1270,** 1–5
40. Shenoy, S. K., Yu, L., and Yu, C. A. (1997) *J. Biol. Chem.* **272,** 17867–17872
41. Hirawake, H., Taniwaki, M., Tamura, A., Amino, H., Tomitsuka, E., and Kita, K. (1999) *Biochim. Biophys. Acta* **1412,** 295–300
42. Baysal, B. E., Ferrell, R. E., Willett-Brozick, J. E., Lawrence, E. C., Myssiorek, D., Bosch, A., van der Mey, A., Taschner, P. E. M., Rubinstein, W. S., Myers, E. N., Richard, C. W. I., Cornelisse, C. J., Devilee, P., and Devlin, B. (2000) *Science* **287,** 848–851
43. Shenoy, S. K., Yu, L., and Yu, C. A. (1999) *J. Biol. Chem.* **274,** 8717–8722
44. Satoh, A., Kim, J.-K., Miyahara, I., Devreese, B., Vandenberghe, I., Hacisalihoglu, A., Okajima, T., Kuroda, S., Adachi, O., Duine, J. A., Van Beeumen, J., Tanizawa, K., and Hirotsu, K. (2002) *J. Biol. Chem.* **277,** 2830–2834
45. Stowell, M., McPhillips, T., Rees, D., Soltis, S., Abresch, E., and Feher, G. (1997) *Science* **276,** 812–816
46. Okamura, M. Y., and Feher, G. (1992) *Annu. Rev. Biochem.* **61,** 861–896
47. Fisher, N., and Rich, P. R. (2000) *J. Mol. Biol.* **296,** 1153–1162
48. Rothery, R. A., Chatterjee, I., Kiema, G., McDermott, M. T., and Weiner, J. H. (1998) *Biochem. J.* **332,** 35–41
49. Matsson, M., Ackrell, B. A. C., Cochran, B., and Hederstedt, L. (1998) *Arch. Microbiol.* **170,** 27–37
50. Bartoschek, S., Johansson, M., Geierstanger, B. H., Okun, J. G., Lancaster, C. R. D., Humpfer, E., Yu, L., Yu, C. A., Griesinger, C., and Brandt, U. (2001) *J. Biol. Chem.* **276,** 35231–35234
51. Ding, H., Moser, C. C., Robertson, D. E., Tokito, M. K., Daldal, F., and Dutton, P. L. (1995) *Biochemistry* **34,** 15979–15996
52. Gutierrez-Cirlos, E. B., and Trumpower, B. L. (2002) *J. Biol. Chem.* **277,** 1195–1202
53. Oyedotun, K. S., and Lemire, B. D. (1999) *J. Biol. Chem.* **274,** 23956–23962
54. Geisler, V., Ullmann, R., and Kröger, A. (1994) *Biochim. Biophys. Acta* **1184,** 219–226
55. Kim, Y. J. (2000) *J. Microbiol. Biotechnol.* **10,** 48–50
56. Kraulis, P. J. (1991) *J. Appl. Crystallogr.* **24,** 946–950
57. Esnouf, R. (1997) *J. Mol. Graph.* **15,** 133–138
58. Merritt, E. A., and Murphy, M. E. P. (1994) *Acta Crystallogr. Sec. D* **50,** 869–873
59. Collins, M. D., and Jones, D. (1981) *Microbiol. Rev.* **45,** 316–354
60. Kleywegt, G. J., and Jones, T. A. (1994) *Acta Crystallogr. Sec. D* **50,** 175–185